Attenuated Total Reflectance Infrared Spectra of Carbonate Minerals, Deconvoluted by Means of q-BWF Functions

International Journal of Sciences

Research Article Volume 13 – September 2024 (09)

Attenuated Total Reflectance Infrared Spectra of Carbonate Minerals, Deconvoluted by Means of q-BWF Functions

Amelia Carolina Sparavigna[1]

[1]Department of Applied Science and Technology, Polytechnic University of Turin, Italy

Abstract: Here we consider some carbonate minerals and their attenuated total reflectance (ATR) infrared spectra, that we can find in RRUFF database. We apply the q-BWF functions to deconvolute the components of the spectra. The q-BWF functions are the asymmetric line shapes that A. C. Sparavigna defined in 2023, to generalize the BWF (Breit-Wigner-Fano) functions. Nearby all the ATR spectra that we will consider are characterized by the presence of a large peak. We will show that, in the case of aragonite and bastnäsite-(Ce), only one q-BWF function is enough for fitting this main peak.

Keywords: Infrared Spectroscopy, ATR Spectroscopy, q-Gaussian Functions, q-BWF Functions

Introduction

The fitting of Raman spectra with q-Gaussian line shapes, which are a generalization of the Lorentzian profile, has been proposed in 2023 by A. C. Sparavigna. The q-Gaussian line shape is a function based on the Tsallis q-form of the exponential function (Tsallis, 1988). This exponential form is characterized by a q-parameter. When q is equal to 2, we have the Lorentzian function. If q is close to 1, we have a Gaussian function. For values of q between 1 and 2, we have a bell-shaped symmetric function with power-law wings ranging from Gaussian to Lorentzian tails. As shown on many occasions, the q-Gaussians are suitable for fitting Raman spectra (from examples proposed in SSRN to the SERS cases, for instance). However, we can define also an asymmetric function, turning the Breit-Wigner-Fano into a q-BWF function (Sparavigna, 2023). Let us write the BWF as follow:

$$\mathrm{BWF}(x) = C\frac{\left[1-\xi\gamma^{1/2}(x-x_o)\right]^2}{\left[1+\gamma(x-x_o)^2\right]}$$

In the function given above, x_o represents the center of the line. When asymmetry parameter ξ is zero, BWF becomes a symmetric Lorentzian function. Note that the center of the line does not correspond to the position of the peak of the function (Ferrari & Robertson, 2000). As in Sparavigna, 2023, we can define the q-BWF function:

$$\text{q-BWF} = C\left[1-\xi\gamma^{1/2}(q-1)^{1/2}(x-x_o)\right]^2\left[1+(q-1)\gamma(x-x_o)^2\right]^{1/(1-q)}$$

In fact, the Lorentzian function is substituted by a q-Gaussian function (see Appendix).

We have already applied the q-BWF functions in some occasions (link1, link2, link3), for the Raman bands of molybdenum disulfide and barium titanate, and for the ATR infrared spectra (Attenuated Total Reflectance) of the barite-group minerals. Here we will consider some carbonate minerals for further investigation of the ATR bands. Let us note that the "reflectance techniques may be used for samples that are difficult to analyze by the conventional transmittance method" (Khoshhesab, 2012). The ATR spectra here analyzed are given by the RRUFF database (Lafuente, 2015). RRUFF database is useful for testing new approaches to the deconvolution of spectra by means of functions which are not included among the line shapes commonly available in curve fitting software (that is, Gaussian, Lorentzian, Voigt, pseudo-Voigt functions). Asymmetric functions are necessary to represent the ATR spectral bands: the asymmetric q-BWF functions are suitable for purpose.

ATR spectral bands

As told by Subramanian and Rodriguez-Saona, 2009, ATR is "one of the most commonly used sampling techniques in recent times". When an IR light beam passes from a medium with a high refractive index into "a medium of low refractive index (sample)", we can observe that "at a particular angle of incidence, almost all the light waves are reflected back. This phenomenon is called total internal reflection. In this condition, some amount of the light energy escapes the crystal and extends a small distance (0.1–5 μm) beyond the surface in the form of waves". These waves are the evanescent waves. "The intensity of the reflected light reduces at this point. This phenomenon is called *attenuated total reflectance*" (Subramanian & Rodriguez-Saona, 2009).

"The partial penetration of the IR light by an evanescent wave allows an absorption spectrum to be recorded" (see for instance, QD-Europe). The penetration depth of the evanescent wave is a

Published at: http://www.ijsciences.com/pub/issue/2024-09/
DOI: 10.18483/ijSci.2803; Online ISSN: 2305-3925; Print ISSN: 2410-4477

Amelia Carolina Sparavigna (Correspondence)
+

function of the angle of incidence at the sample surface interface. "Deeper penetration into a sample is achieved with either a smaller incident angle or a lower refractive index ATR crystal" (QD-Europe). It is stressed that an ATR spectrum is "different to that obtained for the same sample when collected as a transmission spectrum", since measurement methods are different, being differences dictated "by the fundamental way the sample information is being collected". In transmission spectroscopy, the light passes through the sample, "whereas ATR spectroscopy is the interaction of light by passage into the surface of a sample species. *Note that neither method can be regarded as giving the "correct" spectrum – they are simply different*" (QD-Europe). The web site details the role of wavelength and refractive index on the penetration depth of the light. Also, the differences of intensities, the band shift, and the band asymmetries that we observe when an ATR spectrum is compared to a transmission spectrum, are discussed. For instance, regarding the band distortion, it is told that "sometimes in ATR measurements the absorption bands can become *slightly asymmetric* compared to the bands seen in transmission measurements" (QD-Europe). The deformation of the band shape is due to "the rapid change of refractive index of the sample across the band". "The refractive index of the sample varies from a low value on the short wavelength side of the band to a high value on the long wavelength side. This causes the effective penetration depth to also rapidly increase toward the long wavelength side and causes the characteristic shape of the bands seen" (QD-Europe).

Is it possible to compare the IR spectral results? Let us consider the observations made by Kendix, 2009: "in most cases comparison of standard spectra collected in FIR transmission and FIR ATR mode leads to only a few differences. The most obvious, when comparing transmission with ATR, is the distortion of band shape. The ATR band shape appears *asymmetrical* in the lower wavenumber region when compared to spectra collected in transmission mode. Also, *intensity differences* are noticed. However, the biggest difference can be the *shift* of strong absorbing bands moving to lower wavenumbers in ATR mode" (Kendix, 2009). Usually, "the shifts observed are small, approximately 1-10 cm^{-1}, but for very strong absorbing compounds the shifts observed can be as big as 30-50 cm^{-1}" (Kendix, 2009). Then the ATR spectra can be "considerably different from transmission spectra with respect to intensities, band shift and band distortions" (Kendix, 2009). If we could use both techniques, we could obtain databases, for instance, to "identifying unknown pigment samples" (Kendix considers pigments in the framework of analyses of cultural heritage materials). "Perhaps it would be less time consuming and more convenient to try to correct the ATR spectrum to simulate a transmission spectrum by using a correction algorithm" (Kendix, 2009). Besides advanced ATR correction algorithms, we could "try applying the Kramers-Kronig transformation on the ATR spectra". However, "the transformation of spectra are usually problematic". Kendix proposes an example of transformations with algorithm and KK relations on cinnabar ATR spectrum, concluding that it is better to collect both transmission and ATR spectra "to build a database for comparison with unknown samples using both techniques as means of detection and identification".

Then, as given in literature, the ATR measurement method is producing intrinsically asymmetric bands, and therefore, for the deconvolution of the spectrum, an asymmetric band shape is required. We will show that, using the asymmetric q-BWF functions, we can determine the components of ATR spectra, useful for comparison with infrared data available from literature.

RRUFF spectra

The deconvolutions in the following figures are obtained by means of software Fityk (Wojdyr, 2010), after defining in it the q-Gaussian and q-BWF functions (see Appendix for further details). Note that the position of the center of a q-BWF function is different from the position of the peak. In the following tables, we give the position of the peak of components. The infrared spectra are given in RRUFF through the attenuated total reflectance technique. The instrumental settings are according SensIR Durascope on a Nicolet Magna 860 FTIR. We consider some carbonate minerals, given in alphabetic order.

Ankerite R050181 has Ideal Chemistry $Ca(Fe^{2+},Mg)(CO_3)_2$. Source: Marcus Origlieri, Owner: RRUFF. Measured chemistry: $Ca_{1.00}(Fe^{2+}_{0.60}Mg_{0.35}Mn^{2+}_{0.05})_{\Sigma=1}(CO_3)_2$. In the Fig.1, we can see that, for fitting with a lower misfit the largest peak, we need two components. Here we consider both components as being the peak and its shoulder. In Kim et al., 2021, we can find IR data for comparison (samples with different Mg percentage).

Table I: Peaks positions in cm^{-1}

R050181 (Fig.1, right)	725	871	1014	1404	1483	1808
R050181 (Kim et al.)	725	870		1408		
Ank_1 (Kim et al.)	726	873		1416		
Ank_2 (Kim et al.)	726	873		1405		
Ank_3 (Kim et al.)	724	871		1412		
Ank_4 (Kim et al.)	727	874		1419		

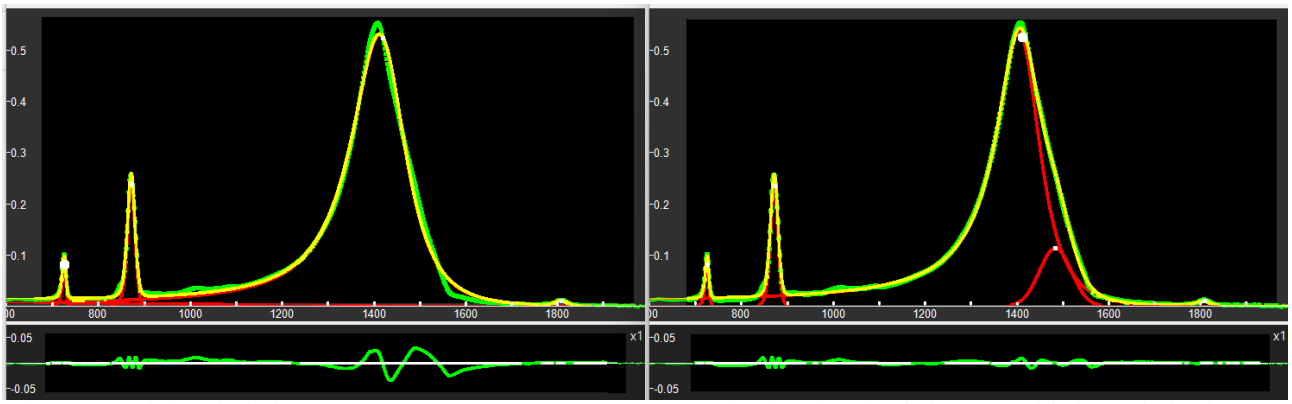

Fig.1: Deconvolution of ankerite RRUFF R050181 ATR spectrum. We use q-BWF functions (in red). The lower part of the images is showing the misfit, that is the difference between data (green) and the sum of components (yellow curve). On the left, one q-BWF component is used for the largest peak. On the right, two q-BWF functions are used for this peak, to reduce the misfit. Consequntly, we have the main component at 1404 cm^{-1}, and its "shoulder" at 1483 cm^{-1}.

Aragonite R040078 has Ideal Chemistry $Ca(CO_3)$. Source is the University of Arizona Mineral Museum, Owner RRUF. The measured chemistry is equal to the ideal one.

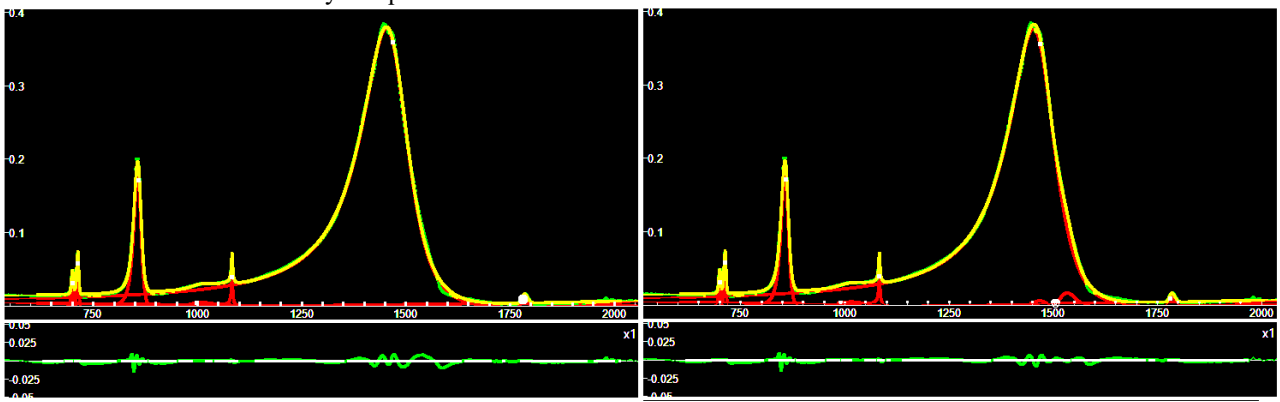

Fig.2: Deconvolution of aragonite RRUFF R040078 ATR spectrum. On the left, one component is used for the main peak. On the right, a second component is added. We can see that this further component has a very small effect. Therefore, we do not consider its presence.

As we can see in the Figure 2, in the case of this aragonite, where the measured chemistry is equal to the ideal chemistry, the largest peak is well described by one q-BWF function. In Chukanov, 2014, we can find the IR transmittance spectrum for comparison.

Table II: Peaks positions in cm^{-1}

R040078	700	713		856	1083	1452		1785
Chukanov	700	713	844	854.5	1083	1470	1533	1785

Bastnäsite-(Ce) R050409 has Ideal Chemistry: $Ce(CO_3)F$. Source: G.R. Rossman, Owner: RRUFF. Measured Chemistry: $(Ce_{0.54}(La,Pr)_{0.25}Nd_{0.21})_{\Sigma=1}CO_3F_{1.00}$. As in the case of aragonite, the fitting of the main peak can be obtained with one q-BWF function. The fit can be improved, with two small further components (see the Fig.3). In Chukanov, 2014, we can find the IR transmittance spectrum for comparison.

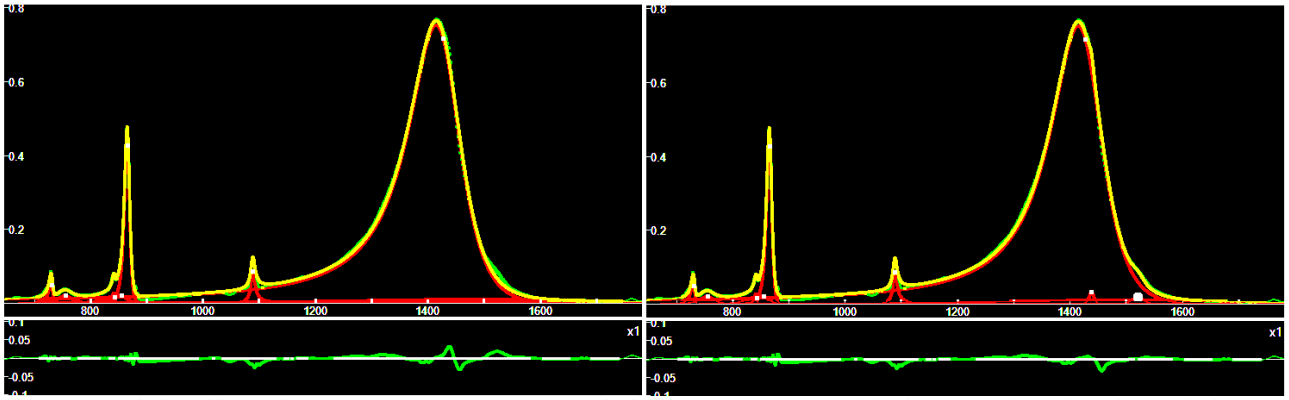

Fig.3: Deconvolution of bastnäsite-(Ce) R050409 ATR spectrum. On the left, one component is used for the main peak. On the right, two further very small components have been added.

Table III: Peaks positions in cm^{-1} ("sh" means "shoulder")

R050409	730	755	841	865	1088	1415	1438	1522	2508
Chukanov	612	694	729	841	867	1085	1417sh	1449	

Calcite has Ideal Chemistry $Ca(CO_3)$. **R040070:** Source: University of Arizona Mineral Museum, Owner: RRUFF. Measured Chemistry: $(Ca_{0.99}Mg_{0.01})CO_3$. **R040170**. Source: University of Arizona Mineral Museum. Owner: RRUFF. Measured Chemistry: $(Ca_{0.99}Mg_{0.01})CO_3$. **R050009.** Source: Eugene Schlepp, Owner: RRUFF. The measured chemistry is equal to the ideal one, with trace amounts of Mn. **R050048**. Source: University of Arizona Mineral Museum. Owner: RRUFF. Measured Chemistry: $(Ca_{0.99}Zn_{0.01})CO_3$. In Gunasekaran et al., 2006, in their Table III, we can find data about limestone provided by the authors, and Raman data from White, 1974, and infrared data from Gaffey, 1986. We can use these data for comparison, as we have already proposed in a previous discussion. In Chukanov, 2014, we can find the IR transmittance spectrum for comparison. Data are also available from Kim et al., 2021.

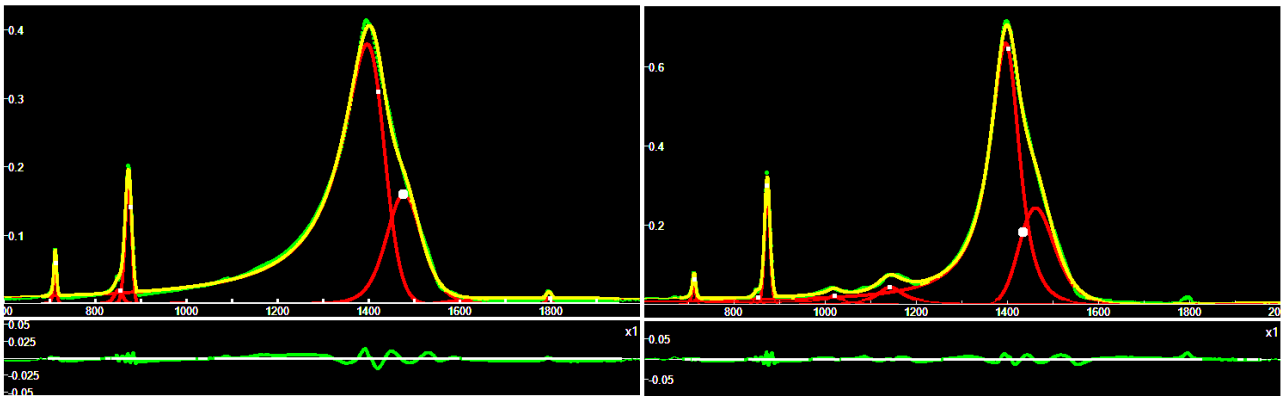

Fig. 4: Deconvolutions of calcite R040070 (on the left) and calcite R040170 (on the right) ATR spectra.

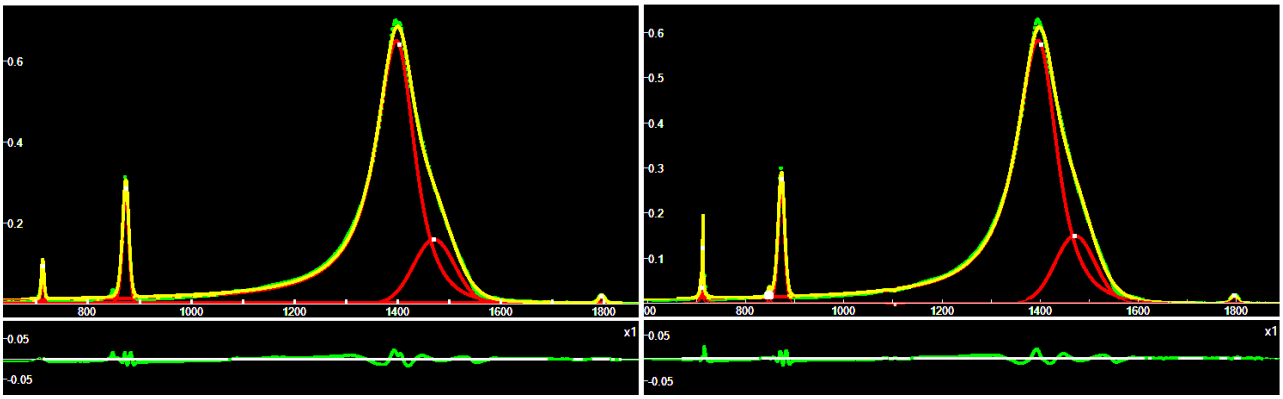

Fig.5: Deconvolutions of calcite R 050009 (on the left) and calcite R050048 (on the right) ATR spectra.

Table IV: Peaks positions in cm^{-1} ("sh" means "shoulder")

R040070	712		851	873		1398	1480	1796	
R040170	713		851	873	1020	1144	1396	1465	1779
R050009		712	848	873	1090		1396	1481	1796
R050048		710 713	848	874			1396	1475	1795
Chukanov		712	847	876			1427	1470sh	1795
Gunasekaran et al.		712		874			1425		1798
Gaffey		712		876			1435		1812
Kim et al., Cal_1		712		872			1395		
Kim et al., Cal_6		713		872			1396		

Dolomite R040030. Ideal Chemistry: $CaMg(CO_3)_2$. Source: University of Arizona Mineral Museum. Owner: RRUFF. Measured Chemistry: $(Ca_{0.99}Mg_{0.01})Mg1_{.00}(CO_3)_2$; trace amounts of Mn. In Chukanov, 2014, we can find the IR transmittance spectrum for comparison. Data are also available from Kim et al., 2021.

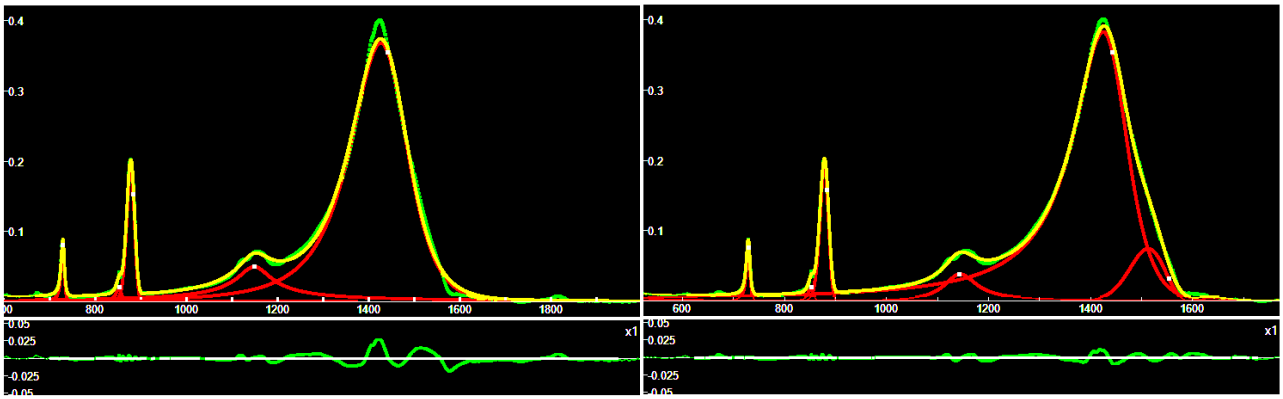

Fig.6: Deconvolution of dolomite R040030 ATR spectrum. On the left, one component is used for the main peak. On the right, a further component has been added.

Table V: Peaks positions in cm^{-1} ("sh" means "shoulder")

R040030	605	671	729		852		878	1120	1160	1424	1518	1815
Chukanov			732	743sh	842	865sh	870	1075		1420	1458	1810
Kim et al., Dol_1			728				877			1418		
Kim et al., Dol_3			729				877			1419		

Gaspéite R040157, Ideal Chemistry: $Ni(CO_3)$. Source: University of Arizona Mineral Museum. Owner: RRUFF. **Huntite R040126**, Ideal Chemistry: $CaMg_3(CO_3)_4$. Source: University of Arizona Mineral Museum. Owner: RRUFF. In Chukanov, 2014, we can find the IR transmittance spectrum of huntite.

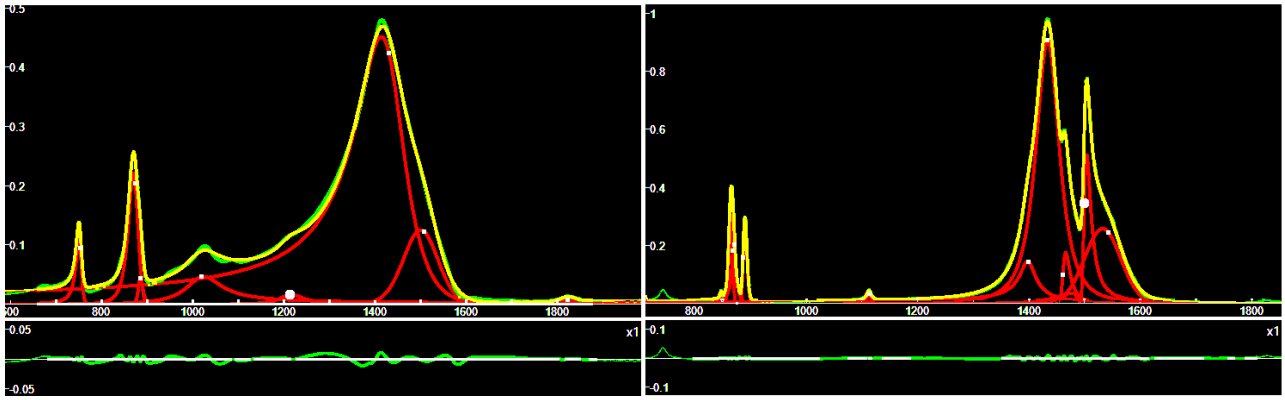

Fig.7: Deconvolutions of gaspéite RRUFF 040157 (left) and huntite R040126 (right) ATR spectra.

Table V: Peaks positions in cm^{-1} ("sh" means "shoulder")

R040126	742	847	864	870	890	1113	1398	1434	1464		1505	1534		1829
Chukanov	742	847		869	879	892	1114			1445	1466	1475sh	1512	1530	1545sh	1825

Magnesite Ideal Chemistry: $Mg(CO_3)$ **R040114**. Source: University of Arizona Mineral Museum, Owner: RRUFF. Measured Chemistry: $(Mg_{0.98}Fe0_{.01})_{C1.00}O_3$. **R050676.** Source: University of Arizona Mineral Museum. Owner: RRUFF. Measured Chemistry: $(Mg_{0.87}Fe^{2+}_{0.12}Ca_{0.01})CO_3$; trace amounts of Mn and Cd.

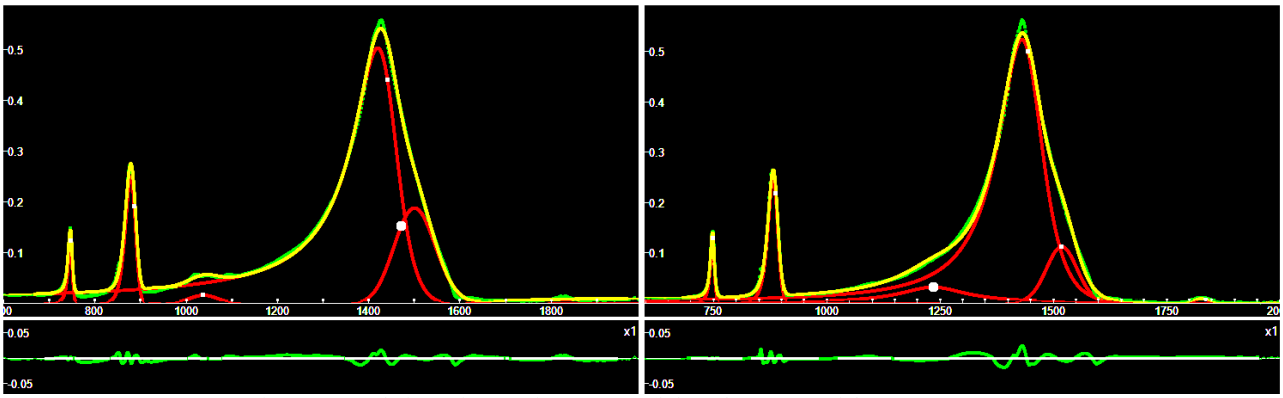

Fig.8: Deconvolutions of magnesite R050676 (left) and R050443 (right) ATR spectra.

Rhodochrosite R050116. Ideal Chemistry: $Mn(CO_3)$. Source: He Xin Jian. Owner: RRUFF. **Siderite R050349**. Ideal Chemistry: $Fe(CO_3)$. Source: California Institute of Technology. Owner: RRUFF. Measured Chemistry: $(Fe_{0.83}Mg_{0.09}Mn_{0.05}Ca_{0.01})CO_3$.

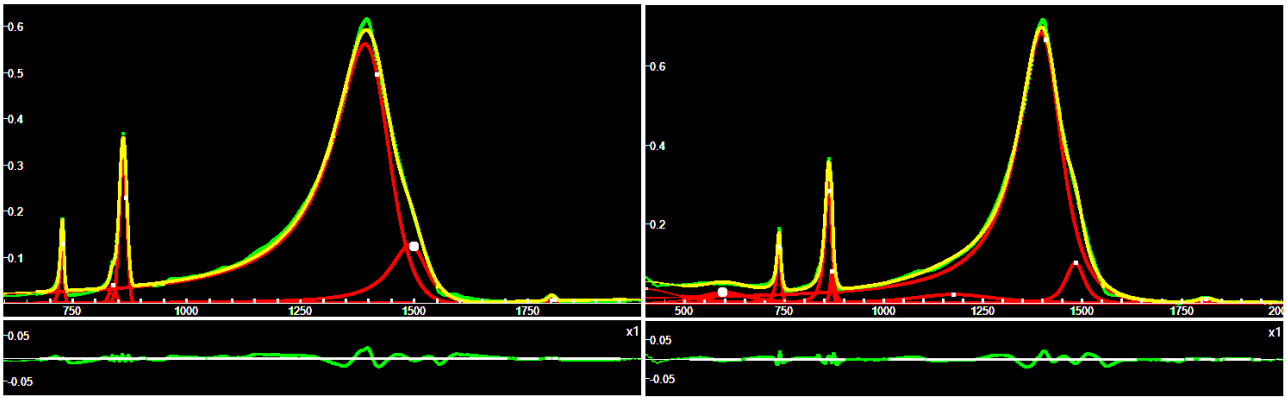

Fig.9: Deconvolutions of rhodochrosite R050116 (left) and siderite R050349 (right) ATR spectra.

Smithsonite R040051. Ideal Chemistry: $Zn(CO_3)$. Source: University of Arizona Mineral Museum. Owner: RRUFF. Measured Chemistry: $(Zn_{0.94}Ca_{0.02}Mg_{0.02})C_{1.01}O_3$. **Strontianite R050564**. Ideal Chemistry: $Sr(CO_3)$ Source: Dave Bunk Minerals. Owner: RRUFF. Measured Chemistry: $(Sr_{0.85}Ca_{0.15})CO_3$.

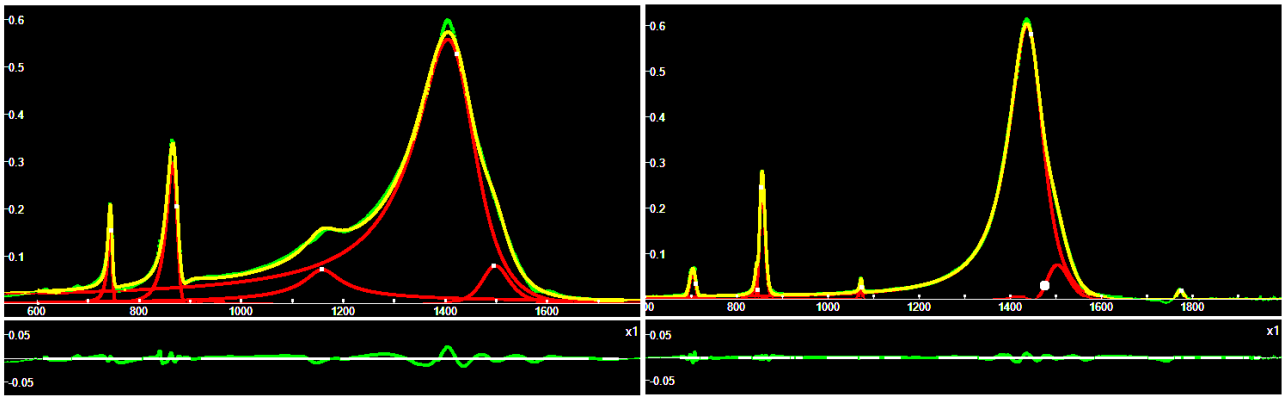

Fig.10: Deconvolutions of smithsonite R040051 (left) and strontianite R050564 (right) ATR spectra.

Witherite R040040. Ideal Chemistry: $Ba(CO_3)$. Source: University of Arizona Mineral Museum. Owner: RRUFF.

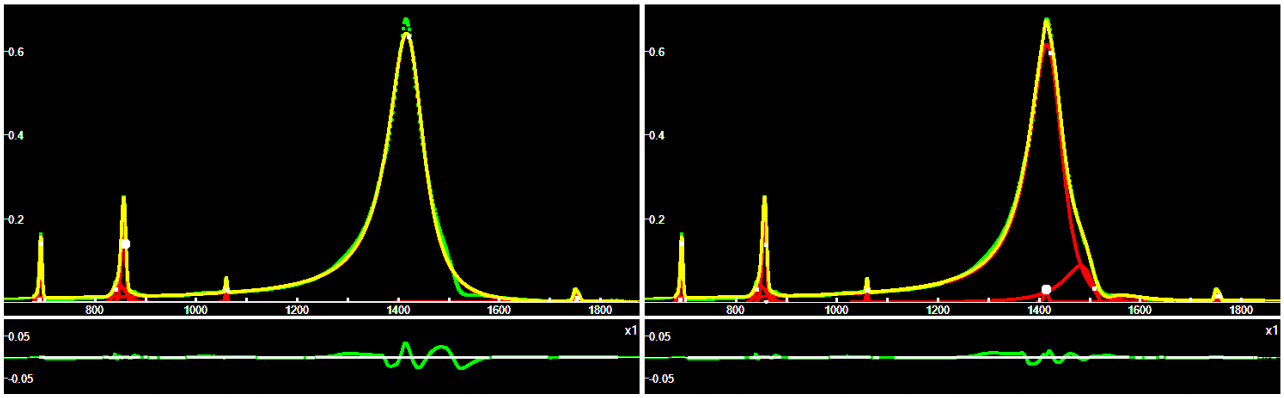

Fig.11: Deconvolution of witherite R040040. On the left, one component is used for the main peak. On the right, two further components have been added.

Discussion

Nearby all the ATR spectra of the carbonate minerals that we have considered are characterized by the presence of a large peak. In the case of aragonite and bastnäsite-(Ce) only one q-BWF function is enough for fitting this peak. In the other cases, besides huntite of course, the main peak is characterized by a large q-BWF component and a shoulder. In the case of calcite, see Table IV, the presence of this shoulder is also evidenced by the transmittance measurements given by Chukanov, 2014.

Appendix – q-Gaussian and q-BWF functions

Sparavigna, 2023, proposed for the first time the use of q-Gaussian function in Raman spectroscopy. She defined also the q-BWF functions which are generalizing the Breit-Wigner-Fano (asymmetric) line shape in the framework of the q-exponential function. Here we show how to apply, by means of Fityk software, the q-Gaussian and the q-BWF functions in spectroscopy. Let us remember that the q-Gaussian functions are probability distributions proper of the Tsallis statistics (Tsallis, 1988, Hanel et al., 2009). The q-Gaussian is defined as: $f(x) = Ce_q(-\beta x^2)$, where $e_q(.)$ is the q-exponential function and C a scale constant (in the exponent, $\beta = 1/(2\sigma^2)$). The q-exponential has expression: $e_q(u) = [1 + (1-q)u]^{1/(1-q)}$. Then, the q-Gaussian function with center of the band at x_o is:

$$q\text{-}Gaussian = Cexp_q(-\beta(x-x_o)^2) = C[1 + (q-1)\beta(x-x_o)^2]^{1/(1-q)}$$

The expression of the q-BWF function has been given in the Introduction.

In Fityk, a q-Gaussian function can be defined in the following manner:

define Qgau(height, center, hwhm, q=1.5) = height*(1+(q-1)*((x-center)/hwhm)^2)^(1/(1-q))

q=1.5 the initial guessed value of the q-parameter. Parameter hwhm is the half width at half maximum of the component. When q=2, the q-Gaussian is a Lorentzian function, that we can find defined in Fityk as:

Lorentzian(height, center, hwhm) = height/(1+((x-center)/hwhm)^2)

When q is close to 1, the q-Gaussian becomes a Gaussian function. The q-BWF can be defined as:

Qbreit(height, center, hwhm, q=1.5, xi=0.1) = (1-xi*(q-1)*(x-center)/hwhm)^2*height*(1+(q-1)^0.5 *((x-center)/hwhm)^2)^(1/(1-q))

And the BWF can be defined as:

Breit(height, center, hwhm, xi=0.1) = (1-xi*(x-center)/hwhm)^2*height/(1+((x-center)/hwhm)^2)

Using +xi instead of -xi does not change the fitting results in Fityk.

References

1. Chukanov, N.V. (2014). IR Spectra of Minerals and Reference Samples Data. Springer Geochemistry/Mineralogy. Springer, Dordrecht. https://doi.org/10.1007/978-94-007-7128-4_2
2. Ferrari, A. C., & Robertson, J. (2000). Interpretation of Raman spectra of disordered and amorphous
3. carbon. Physical Review B 61: 14095–14107.
4. Gaffey, S. J. (1986). Spectral reflectance of carbonate minerals in the visible and near infrared (0.35-2.55 microns); calcite, aragonite, and dolomite. American Mineralogist, 71(1-2), 151-162.
5. Gunasekaran, S., Anbalagan, G., & Pandi, S. (2006). Raman and infrared spectra of carbonates of calcite structure. Journal of Raman Spectroscopy: An International Journal for Original Work in all Aspects of Raman Spectroscopy, Including Higher Order Processes, and also Brillouin and Rayleigh Scattering, 37(9), 892-899.
6. Hanel, R., Thurner, S., & Tsallis, C. (2009). Limit distributions of scale-invariant probabilistic models of correlated random variables with the q-Gaussian as an explicit example. The European Physical Journal B, 72(2), 263.
7. Kendix, E. L. (2009). Trasmission and Reflection (ATR) Far-Infrared Spectroscopy Applied in the Analysis of Cultural Heritage Materials. Ph.D. Thesis, Alma Mater Studiorum Università di Bologna, Bologna, Italy.
8. Khoshhesab, Z. M. (2012). Reflectance IR spectroscopy. Infrared spectroscopy-Materials science, engineering and technology, 11, 233-244.
9. Kim, Y., Caumon, M. C., Barres, O., Sall, A., & Cauzid, J. (2021). Identification and composition of carbonate minerals of the calcite structure by Raman and infrared

spectroscopies using portable devices. Spectrochimica Acta Part A: Molecular and Biomolecular Spectroscopy, 261, 119980.
10. Lafuente, B., Downs, R. T., Yang, H., & Stone, N. (2015). 1. The power of databases: The RRUFF project. In Highlights in mineralogical crystallography (pp. 1-30). De Gruyter (O).
11. Sparavigna, A. C. (2023). q-Gaussian Tsallis Line Shapes and Raman Spectral Bands. Int. J. Sciences, 12(3), 27-40. https://doi.org/10.18483/ijsci.2671
12. Sparavigna, A. C. (2023). q-Gaussian Tsallis Line Shapes for Raman Spectroscopy (June 7, 2023). Available at SSRN: https://ssrn.com/abstract=4445044 or http://dx.doi.org/10.2139/ssrn.4445044
13. Sparavigna, A. C. (2023). Asymmetric q-Gaussian functions generalizing the Breit-Wigner-Fano functions. Zenodo. https://doi.org/10.5281/zenodo.8356165
14. Sparavigna, A. C. (2023). SERS Spectral Bands of L-Cysteine, Cysteamine and Homocysteine Fitted by Tsallis q-Gaussian Functions. Int. J. Sciences, 12(09), 14-24. http://dx.doi.org/10.18483/ijSci.2721
15. Sparavigna, A. C. (2024). Molybdenum Disulfide MoS2 and the q-BWF line shapes (Raman Spectroscopy). ChemRxiv. doi:10.26434/chemrxiv-2024-cprs3-v3
16. Sparavigna, A. C. (2024). Barium Titanate BaTiO3 Raman Spectra and their deconvolution with q-BWF functions. ChemRxiv. doi:10.26434/chemrxiv-2024-dchgr
17. Sparavigna, A. C. (2024). q-Gaussian and q-BWF functions for the deconvolution of Raman and infrared spectra of Calcite. ChemRxiv. doi:10.26434/chemrxiv-2024-nsmch
18. Sparavigna, A. C. (2024). q-BWF functions to deconvolute the attenuated total reflectance infrared spectra of the barite-group minerals. ChemRxiv. doi:10.26434/chemrxiv-2024-9x1jz
19. Subramanian, A., & Rodriguez-Saona, L. (2009). Chapter 7-Fourier Transform Infrared (FTIR) Spectroscopy, in Infrared Spectroscopy for Food Quality Analysis and Control, D. Sun, Ed.
20. Tsallis, C. (1988). Possible generalization of Boltzmann-Gibbs statistics. Journal of statistical physics, 52, 479-487.
21. White, F. (1974). The Infrared Spectra of Minerals, Farmer V.C. ed., Mineralogical society monograph, 4, 331-363.
22. Wojdyr, M. (2010). Fityk: a general-purpose peak fitting program. Journal of applied crystallography, 43(5), 1126-1128.